Mechanistic Modeling Identifies Drug-Uptake History as Predictor of Tumor Drug Resistance and Nano-Carrier-Mediated Response

Jennifer Pascal,[†,■] Carlee E. Ashley,[‡,#,■] Zhihui Wang,[†,■] Terisse A. Brocato,[⊥] Joseph D. Butner,[⊥] Eric C. Carnes,[§,⊥,#] Eugene J. Koay,[∥,◆] C. Jeffrey Brinker,[⊥,¶,#,▽,○,*] and Vittorio Cristini[†,⊥,#,*]

[†]Department of Pathology, [#]Cancer Research and Treatment Center, and [▽]Department of Molecular Genetics and Microbiology, The University of New Mexico Health Sciences Center, Albuquerque, New Mexico 87131, United States, [‡]Biotechnology and Bioengineering Department, Sandia National Laboratories, Livermore, California 94551-0969, United States, [§]Nanobiology Department, and [○]Self-Assembled Materials Department, Sandia National Laboratories, Albuquerque, New Mexico 87185-1349, United States, [⊥]Department of Chemical and Nuclear Engineering and Center for Biomedical Engineering, and [¶]Center for Micro-Engineered Materials, The University of New Mexico, Albuquerque, New Mexico 87131, United States, [∥]Department of Radiation Oncology, The University of Texas MD Anderson Cancer Center, Houston, Texas 77030, United States, and [◆]Department of Nanomedicine, Houston Methodist Research Institute, Houston, Texas 77030, United States. [■]These authors contributed equally.

ABSTRACT A quantitative understanding of the advantages of nanoparticle-based drug delivery *vis-à-vis* conventional free drug chemotherapy has yet to be established for cancer or other diseases despite numerous investigations. Here, we employ first-principles cell biophysics, drug pharmaco-kinetics, and drug pharmaco-dynamics to model the delivery of doxorubicin (DOX) to hepatocellular carcinoma (HCC) tumor cells and predict the resultant experimental cytotoxicity data. The fundamental, mechanistic hypothesis of our mathematical model is that the integrated history of drug uptake by the cells over time of exposure, which sets the cell death rate parameter, and the uptake rate are the sole determinants of the dose response relationship. A universal solution of the model equations is capable of predicting the entire, nonlinear dose response of the cells to any drug concentration based on just two separate measurements of these cellular parameters. This analysis reveals that nanocarrier-mediated delivery overcomes resistance to the free drug because of improved cellular uptake rates, and that dose response curves to nanocarrier mediated drug delivery are equivalent to those for free-drug, but "shifted to the left;" that is, lower amounts of drug achieve the same cell kill. We then demonstrate the model's general applicability to different tumor and drug types, and cell-exposure time courses by investigating HCC cells exposed to cisplatin and 5-fluorouracil, breast cancer MCF-7 cells exposed to DOX, and pancreatic adenocarcinoma PANC-1 cells exposed to gemcitabine. The model will help in the optimal design of nanocarriers for clinical applications and improve the current, largely empirical understanding of *in vivo* drug transport and tumor response.

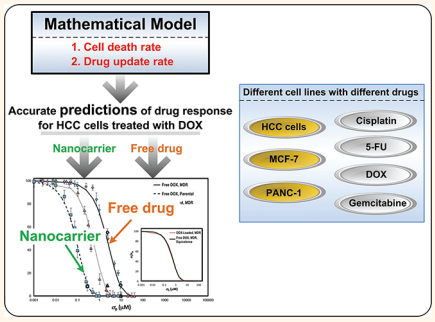

KEYWORDS: drug delivery · mathematical modeling · mesoporous silica nanoparticle · pharmacokinetics–pharmacodynamics model · protocells

Stable nanoparticles capable of specifically binding to cancer cells and delivering high doses of therapeutic compounds could be transformational for cancer therapy by more efficiently delivering drugs into cancer cells, while simultaneously reducing toxic side effects in healthy cells and tissues.[1−3] An ideal targeted nanoparticle drug carrier, or "nanocarrier," should have (i) the capacity for carrying high levels of multiple diverse molecular cargos, for example, small molecules, drugs, siRNAs, peptides, and imaging agents; (ii) the ability to reside in the blood for extended periods without elimination by the immune or excretory systems; and (iii) the specificity for binding only to targeted disease cells (either endothelium or epithelium), while avoiding normal, healthy cells. To achieve these combined features, we have recently developed a modular, composite nanocarrier termed a "protocell" (Figure 1).[4−6] Protocells synergistically combine the advantages of liposomes (low inherent toxicity, immunogenicity, and long circulation times) and

* Address correspondence to VCristini@salud.unm.edu, cjbrink@sandia.gov.

Received for review September 18, 2013 and accepted November 4, 2013.

Published online November 04, 2013
10.1021/nn4048974

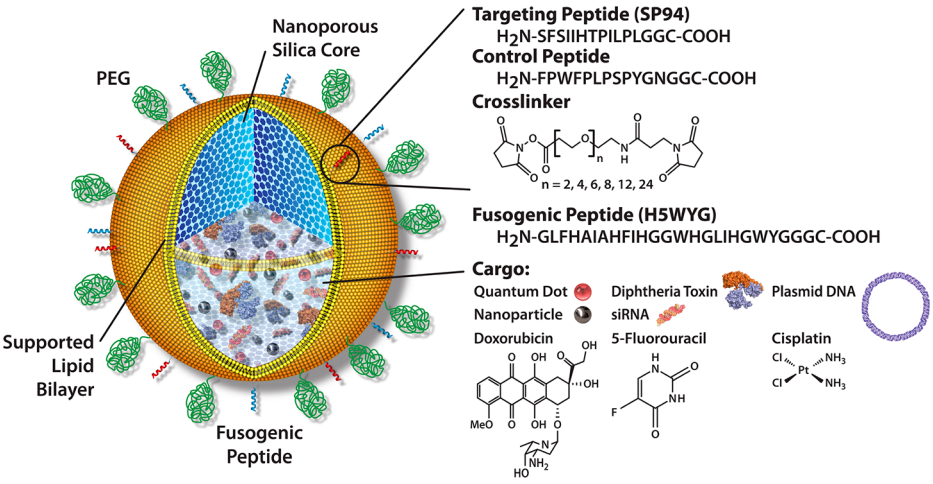

Figure 1. Protocell design. Nanoporous silica cores are loaded with multiple drug cargos by adsorption to the high surface area silica matrix. The drug-loaded core is then enveloped by a single lipid bilayer, which is further functionalized with (1) polyethylene glycol (PEG) to reduce nonspecific interactions with its environment; (2) targeting peptides to direct protocell binding to specific cells; and (3) pH-responsive peptides which cause disruption of endosomes and the bilayer coating upon particle internalization into acidic intracellular compartments, allowing drug delivery into the cytosol of the target cell.

porous nanoparticles (stability and an enormous capacity for simultaneous delivery of multiple cargos). We have demonstrated that protocells have a 100-fold greater specificity in target-cell binding than equivalent fluid-phase liposomes.[4] Furthermore, using a model of hepatocellular carcinoma (HCC), we demonstrated that protocells carrying a cocktail of doxorubicin (DOX), 5-FU, and cisplatin were so potent that a single targeted protocell could kill a multidrug-resistant hepatocellular carcinoma cell *in vitro*, while sparing normal hepatocytes.[4]

Here, using a mathematical modeling framework based on first principles of drug and cell mass conservation, with biophysical parameters describing cellular uptake rates of the drug/nanoparticle and cellular death rates, we accurately predict the dose response of HCC to DOX, 5-FU, and cisplatin administered as free drugs or loaded into protocells, and provide mechanistic understanding of the observed increased efficiency and efficacy of targeted nanoparticle-based delivery compared to that of the free drug. In particular, delivery of DOX using protocells was found to kill higher numbers of cells in a colony than the delivery of free DOX due to increased uptake rates by cells in nanocarrier-mediated delivery and mitigation of drug loss by MDR efflux pumps such as P-glycoprotein (Pgp).

The integrative research studying cellular response to both free and nanoparticle-delivered chemotherapeutic drugs has so far focused on one particular aspect of response, such as the dose response curve or the pharmacokinetics–pharmacodynamics of a particular drug.[7−10] The area under the concentration *versus* time curve (AUC) has been the major predictor of anticancer agent effects on cell death. The survival of cells relative to controls, when plotted against either the extracellular AUC or C^aT (where C is concentration of drug, T is exposure time and a is a constant dependent on tumor type), yields a nonlinear, sigmoidal curve that can be typically described by the Hill model.[7] In line with these phenomenological approaches, many *ad-hoc* modifications have been made to the Hill model to describe dose response curves obtained from *in vitro* cytotoxicity experiments, including examining the shape of the concentration-*versus*-time curve and exploring how cell damage is affected or determined by drug accumulation within the cells.[10,11] However, the Hill-type models do not allow one to predict how features like the duration of drug exposure (a crucial factor in determining the shape of the dose response curve) affect cell kill. To address this problem, various mechanistic models have been developed, including exponential kill models[9] and other types of models[7,8,12−16] that rely on compartmental models of drug action. However, these models require measurements of many biological properties of tumor cells and drugs (*e.g.*, cell cycle phase specificity, cell cycle time, and the level of drug resistance), making them difficult to use in predicting dose response curves.

Here, we use an integrated experimental and mathematical modeling approach, which builds on our prior efforts,[17,18] to study and quantify *in vitro* tumor drug response. Using experimental cytotoxicity data, we develop a simple yet mechanistic mathematical model from first principles, coupling the cell and drug dynamics, and fit this model to the data to obtain parameters describing cellular uptake of—and response to—the drug. We demonstrate that the cell death rate is a universal mechanistic, predictable function of the time-integral of drug exposure, replacing the unnecessarily complicated and *ad-hoc* phenomenological models of cell death described above.[8,9,16]

Furthermore, after calibrating the model using just two drug concentration data points, we accurately predict the nonlinear dose response curves for all drug concentrations and for both types of delivery methods, that is, free drug and drug-loaded protocells, to both drug sensitive and resistant HCC cell types. We then demonstrate the general applicability of the model formulation to different cell/drug types, delivery vehicles, and time courses. These differences are simply and uniquely accounted for by different values of two fundamental parameters, cell death and drug uptake rates.

RESULTS AND DISCUSSION

Mathematical Model. We performed a set of monolayer *in vitro* assays (see Materials and Methods) where the dynamics of viable cells (change in viable population of cells over time due to drug uptake) and drug (change in drug concentration over time due to uptake by cells) were interdependent. Thus, we developed a mathematical model, from first principles of cell and drug mass conservation, which describes the dynamics of the viable population of cells as a function of drug concentration and the history of drug uptake by the cells. (See Supporting Information *Text* for details and formulation.) Below, we report the solutions describing the changes in viable cell population and drug concentration over time for the three scenarios considered in the experiments.

Scenario 1: Continuous Drug-Exposure Model. Defining the dimensionless variables, $\hat{n} = n/n_0$, $\hat{\sigma} = \sigma/\sigma_0$, $\hat{t} = \lambda n_o t$, equations S1−S4 (Supporting Information *Text*) leads to semianalytical implicit solutions for drug and cell concentrations $\hat{\sigma}$ and $\hat{n}$ as a function of time $\hat{t}$:

$$\hat{t} = -\int_1^{\hat{\sigma}} \frac{d\hat{\sigma}'}{\hat{\sigma}'(1+\Phi(1-\hat{\sigma}'+\ln\hat{\sigma}'))}$$
$$\hat{n} = 1+\Phi(1-\hat{\sigma}+\ln\hat{\sigma}) \qquad (1a,b)$$

where σ_0 and n_0 are initial drug and cell concentrations and λ is the specific rate of uptake of drug (by a unit concentration of cells). The dimensionless constant $\Phi = (\lambda_A\sigma_0)/(\lambda n_0)$ is the ratio between the characteristic time scales associated with cell death and drug uptake by the cells.

Scenario 2: Discontinuous Drug-Exposure Model. If drug exposure in the above scenario is discontinued at $\hat{t} = \hat{t}_d$, eq 1a,b is only valid for $\hat{t} < \hat{t}_d$, that is, while drug is delivered continuously to the cells. It is straightforward to demonstrate that, for $\hat{t} > \hat{t}_d$, eq 1a,b can be replaced by (eqs S5 and S6, Supporting Information *Text*):

$\hat{t} > \hat{t}_d$:

$$\hat{n} = \hat{n}(\hat{t}_d)\, e^{-\Phi(1-\hat{\sigma}(\hat{t}_d))(\hat{t}-\hat{t}_d)} \quad \text{and } \sigma = 0 \qquad (2a,b)$$

where $\hat{n}(\hat{t}_d)$ and $\hat{\sigma}(\hat{t}_d)$ are the concentrations of viable cells and of drug, calculated from eq 1a,b at $\hat{t} = \hat{t}_d$. Equation 2a,b describes apoptosis of cells in the colony at an exponential rate set by the total uptake of drug $\sigma_0 - \sigma(\hat{t}_d)$ that has occurred up to time $\hat{t} = \hat{t}_d$.

Scenario 3: Constant Drug-Concentration Model. For experimental conditions simulating constant drug concentration $\hat{\sigma}(\hat{t}) = 1$, eqs S7, S8 lead to the solution (Supporting Information *Text*):

$$\hat{\sigma}_u = (\Phi/2)^{-1/2}\tanh((\Phi/2)^{1/2}\hat{t});$$
$$\hat{n} = 4\frac{e^{(2\Phi)^{1/2}\hat{t}}}{(e^{(2\Phi)^{1/2}\hat{t}}+1)^2} \qquad (3a,b)$$

where $\hat{\sigma}(\hat{t})$ is total concentration of drug taken up from time 0 to time $\hat{t}$.

Analysis of Coupled Cell and Drug Dynamics. Asymptotic behaviors of eq 1a,b can be found for short and long drug exposure times, respectively (in dimensional variables):

$\lambda n_0 t \ll 1$:

$$\frac{n}{n_0} \approx 1 - \frac{1}{2}\lambda_A\sigma_0\lambda n_0 t^2, \quad \text{and } \frac{\sigma}{\sigma_0} = e^{-\lambda n_0 t} \qquad (4a)$$

$\lambda n_0 t \gg 1$:

$$\frac{n}{n_0} \sim e^{-\lambda_A(\sigma_0-\sigma_\infty)t} \quad \text{and } \sigma \approx \sigma_\infty \qquad (4b)$$

where σ_∞ is the drug concentration value as time t goes to infinity and drug uptake by the cells is completed, and is calculated from eq 1b with $n = 0$. On the basis of the model assumptions, eq 4a reveals that the cells initially uptake drug, thus decreasing drug concentration over time at an exponential rate λn_0. As the drug concentration tends to a constant long-time value σ_∞, cells begin to die. At large times, cell death is exponential, with death rate $\lambda_A(\sigma_0 - \sigma_\infty)$ linearly proportional to the total amount of drug $\sigma_0 - \sigma_\infty$ that the cells have taken up (total uptake). Similar cell viability dynamics occur for discontinuous (eq 2) and constant (eq 3) drug exposure.

Analysis of Cellular Biology Parameters. The parameter values obtained from the fits of the mathematical model to the experimental data (Figure 2; Materials and Methods) are reported in Figure 3 *versus* initial DOX concentration σ_0 in the medium for drug sensitive and resistant HCC cell lines (Table S1, Supporting Information *Text*). Because the drug is packaged at high concentration within the protocell carrier, the effective uptake rates λn_0 of drug by the cells are higher for protocell-based delivery than for free drug delivery (Figure 3A) with the same total amount of drug administered in the medium. The uptake rates are independent (within error) of initial DOX concentration σ_0 (and roughly on cell line) for both methods of delivery. The total amount of DOX, that is, $\sigma_0 - \sigma_\infty$, taken up by the cells (inset) increases as expected with initial DOX concentration σ_0, and is higher for protocell-based delivery than free-drug delivery.

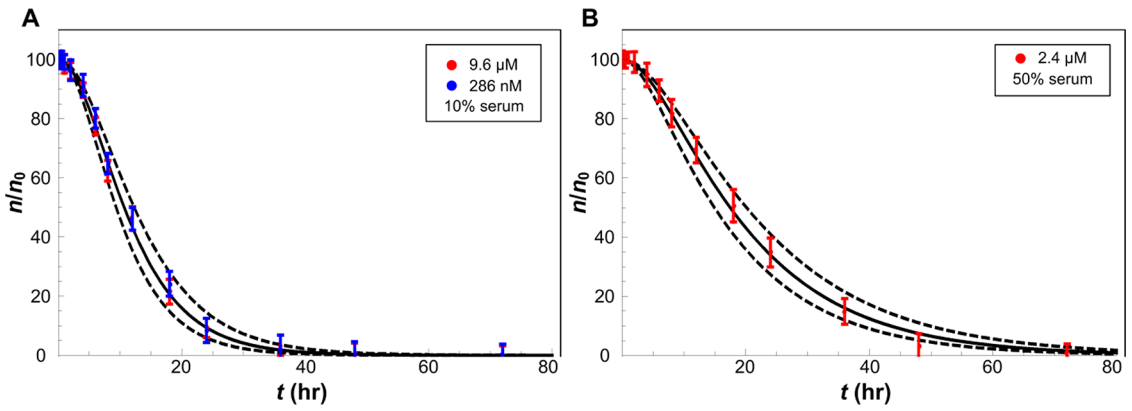

Figure 2. Sample fits of eq 1 (solid curves) to cytotoxicity data (symbols: fraction of viable cells n/n_0 with S.D.) at different drug concentrations, used to calculate mean values of drug-uptake rate and cell-death rate parameters. (A) Drug resistant (red; initial DOX concentration σ_0= 9.6 μM) and sensitive (blue; σ_0= 286 nM) HCC cell lines exposed to free DOX. (B) Drug resistant HCC cells (red; σ_0= 2.4 μM) exposed to DOX-loaded protocells. Additional fits to upper and lower bounds of the experimental measurements (dashed) were used to calculate standard deviations of the parameters (Supporting Information, Tables S1,S2; *Text*).

The long-time death rates $\lambda_A(\sigma_0 - \sigma_\infty)$ for the drug sensitive and resistant cell lines (Figure 3B) increase with initial DOX concentration σ_0 for both methods of delivery. The protocell delivery of DOX leads to higher death rates than those corresponding to free-drug delivery, especially for MDR cells. The results also suggest that for the cells and drug considered here, serum percentage has a negative effect on death rate, which could be a result of protein association with the supported lipid bilayer (Figure 1) of the protocell causing modest leakage of DOX. Moreover, the specific death rates λ_A for both drug resistant and sensitive cell lines are independent (within error) of the method of delivery and initial DOX concentration σ_0 (inset). This supports the model hypothesis (Supporting Information, eq. S3, *Text*) that a linear long-time death rate $\lambda_A(\sigma_0 - \sigma_\infty)$ proportional to the total uptake of drug is sufficient to capture the behavior of the cells, at least within the range of drug concentrations studied here, without the use of unnecessarily complicated models of cell death.[8,9,16] Altogether, these results imply that the protocell-based delivery is more efficient and effective at killing cells than free-drug.

Test of the Time-Dependent Model. As a first test of model predictivity, we investigated the effect of the duration of cell exposure to DOX on cell death (Figure 4) by using experimental data corresponding to delivery for 4 h only to MDR HCC cell lines *via* both free DOX and DOX-loaded protocells at two initial DOX concentrations σ_0. We applied the mathematical model eq 2a,b with t_d = 4 h. We kept the values of the parameters λn_0 and λ_A the same as previously calculated from the corresponding continuous DOX-exposure experiments (Figure 3; Supporting Information, Table S1, *Text*), since according to the model assumptions these parameters are intrinsic properties of the cells independent of the time-delivery protocol. The curves predicted by the mathematical model agree (Figure 4) with the data corresponding to 4 h drug exposure (coefficients of determination R^2 = 0.988 and 0.982 for the free DOX and DOX-loaded 4 h-exposure curves at an initial DOX concentration σ_0 = 92.5 nM; and R^2 = 0.995 and 0.973 for σ_0 = 298 nM), thus validating the model assumptions and equations. When drug is delivered for 4 h only, cells begin to regrow with a doubling time of mitosis of about 25−32 h while at the same time the kill effect of the drug declines; thus, we do not expect the parameters of the model to accurately predict cell viability values for times longer than this doubling time. Consistent with the mathematical model, continuous delivery leads to higher total uptake; that is $\sigma_0 - \sigma_\infty > \sigma_0 - \sigma(4\text{ h})$, because $\sigma(4\text{ h}) > \sigma_\infty$, and thus higher death rates and total death are achieved. This result is consistent with the observation that the uptake time scale 2 h < $(\lambda n_0)^{-1}$ < 15 h, and thus after 4 h the drug uptake process is typically far from being completed.

General Applicability of the Model. We tested the generality of the model by applying it to continuous time-exposure experiments of HCC cells to different drug types, that is, cisplatin (cis) and fluorouracil (5-FU). The long-time death rates $\lambda_A(\sigma_0 - \sigma_\infty)$ and specific death rates λ_A for cis and 5-FU were obtained for both parental and MDR HCC cell lines at a single value of initial drug concentration σ_0, and are independent of delivery methods and cell line (within error) (Supporting Information, Table S2, *Text*). The uptake rates of drug by the cells λn_0 and total amount of drug taken up by the cells $\sigma_0 - \sigma_\infty$ for cis and 5-FU are also roughly insensitive to the delivery method and cell line (within error). Therefore, *in vitro*, there is no apparent advantage in using protocells to deliver cis and 5-FU to HCC cells in contrast to the case for DOX (Figure 3). These observations are consistent with the MDR cell line remaining sensitive to cis and 5-FU, which are not substrates for P-glycoprotein (P-gp; a transporter that transports substrates across extra- and intracellular membranes), and with the fact that cis and 5-FU

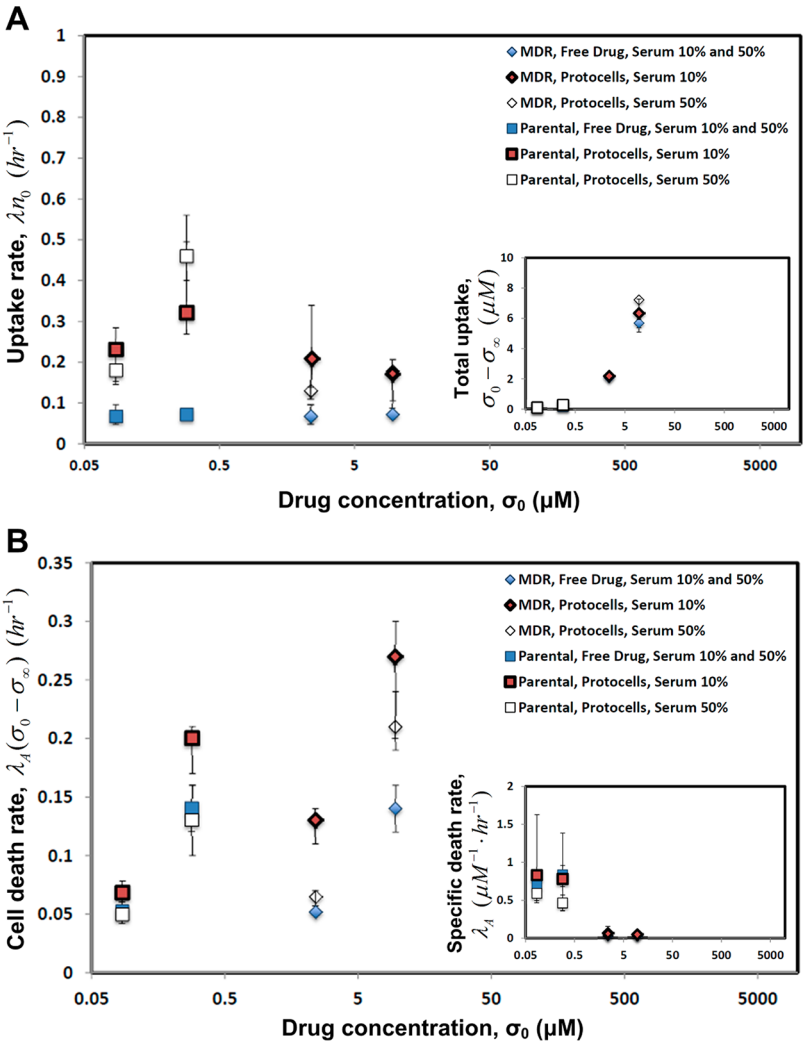

Figure 3. DOX-loaded protocell delivery (red and white symbols with S.D.) leads to higher uptake rates and thus higher rates of cell death compared to free DOX (blue). (A) Uptake rate λn_0 by drug-resistant (MDR, diamonds) and sensitive (parental, squares) HCC cell lines. Inset: total uptake of drug $\sigma_0 - \sigma_\infty$, that is, the difference between initial and long-time drug concentrations in the medium. (B) Long-time cell death rate $\lambda_A(\sigma_0 - \sigma_\infty)$, established in the colony after total drug uptake $\sigma_0 - \sigma_\infty$ has occurred. Inset: specific death rate λ_A, that is, the death rate per unit concentration of drug uptaken. The parameters were calculated by fitting eq 1 to the time-dependent cytotoxicity data (e.g., see Figure 2). For protocells, initial DOX concentration σ_0 is the product of the concentration of protocells in the medium times the average concentration of drug in protocells. σ_0= 2.4 and 9.6 μM (MDR cells), and 0.0857 and 0.286 μM (sensitive).

administered in dimethyl sulfoxide (DMSO) can diffuse readily into cells. However this DMSO delivery approach cannot be used *in vivo* or in human patients, so it is reasonable to expect that there may be an advantage of using protocell-mediated delivery in a clinical setting. Note finally that the model correctly predicts lower uptake for these drugs than for DOX when protocells are used, which is consistent with the observation that the former drugs are loaded at lower concentration than DOX in the protocells.

We then tested applicability to different cell types, by revisiting our *in vitro* experiments[17] with continuous delivery of free DOX to MCF-7 breast cancer cell lines. By fitting the numerical solution of eq 1 at t = 96 h to the dose response data at several initial drug concentrations σ_0 for MDR and parental MCF-7 cells (Supporting Information, Figure S1A, *Text*), we obtained the parameter values: λn_0 = 0.1 h^{-1} and λ_A = 0.08 h^{-1} μM^{-1} (MDR); λn_0 = 0.07 h^{-1} and λ_A = 0.4 h^{-1} μM^{-1} (parental). The coefficients of determination for the fits were R^2 = 0.98 (MDR) and 0.94 (parental). These parameter values are similar to those found for HCC cells (parental) and larger for MDR MCF-7 than MDR HCC, which is consistent with the observation that smaller values of σ_0 are necessary to achieve the same kill in MDR MCF-7 than MDR HCC cells.

Finally, we tested the model on a different cell type and drug, that is, on human pancreatic adenocarcinoma cells continuously exposed to free gemcitabine, as well as to constant gemcitabine concentration (Materials and Methods). By fitting the numerical solution of eq 1 (continuous exposure) and eq 3 (constant exposure)

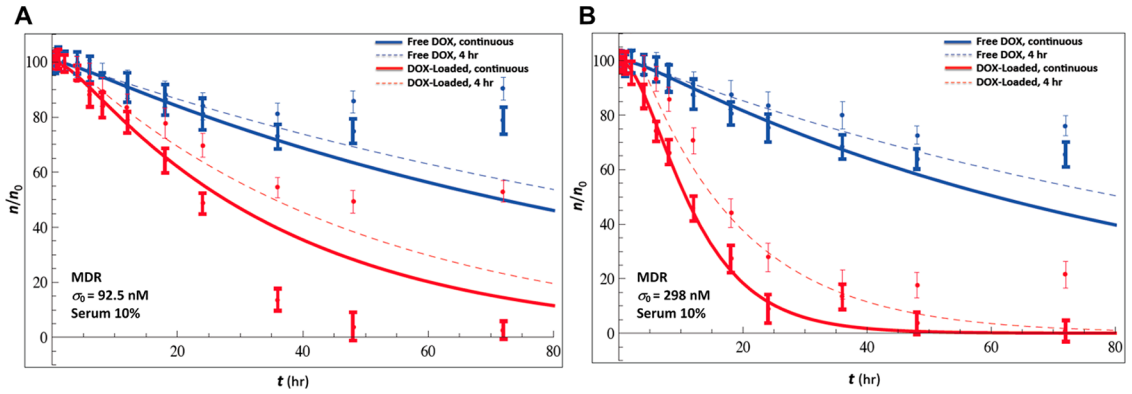

Figure 4. Continuous delivery of DOX over time (thick symbols and solid lines) leads to higher long-time death rates compared to delivery for 4 h (thin symbols and dashed lines). The percentage of viable cells n/n_0 versus time t (symbols with S.D.) for free DOX (blue) and DOX-loaded protocells (red) delivered for 4 h and continuously for 72 h to MDR HCC cell lines; 10% serum; eq 1 (thick lines) and eq 2 (dashed lines). Initial DOX concentrations σ_0 = 0.0925 μM (A) and 0.298 μM (B). The mathematical model, with parameters calibrated from the continuous-drug exposure experiments, is predictive of the viability corresponding to the 4-h exposure experiments. The increase in viability observed at long times (symbols) is due to resumed proliferation and not accounted for in the mathematical model of cell kill.

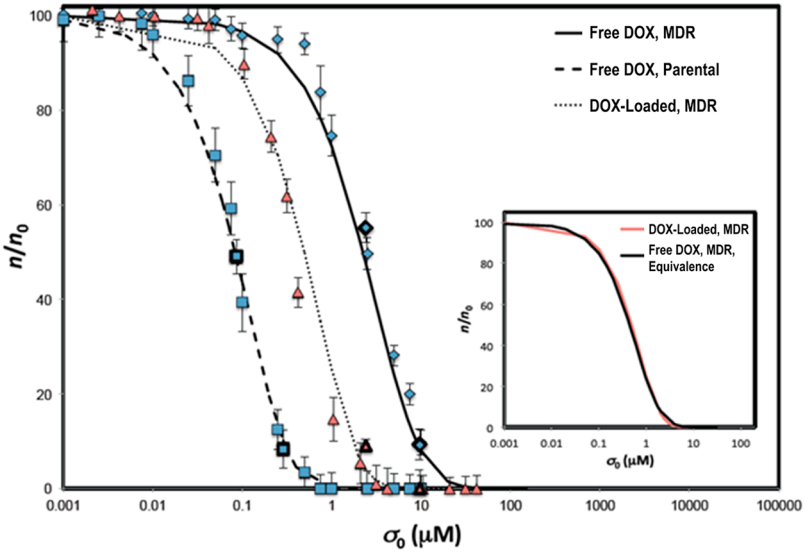

Figure 5. Mathematical model predicts dose–response curves. Numerical integration of eq 1 at t = 24 h (solid, dashed, and dotted curves) and experimental cytotoxicity data (symbols with S.D.): free DOX (blue squares, parental; diamonds, MDR); DOX-loaded protocells (red). R^2 = 0.987 (MDR, free DOX), 0.991 (MDR, DOX-loaded protocells), and 0.996 (parental, free DOX). For prediction of each dose–response curve, a single value of drug uptake rate λn_0 and specific cell death rate λ_A parameters was calculated (Materials and Methods; Supporting Information, Table S1, *Text*) by fitting eq 1 to time-course viability data at two drug concentrations (dark-outlined symbols), and then averaging the two resulting values for each parameter. Inset: "equivalence" between free-DOX and DOX-loaded-protocell dose–response is demonstrated by superposing least-squares fits (R^2 = 0.999) through the two data sets (by rescaling the free-drug concentration by a factor of 1/5 determined empirically).

at t = 96 h (Supporting Information, Figure S1B, *Text*), we found the parameter values: λn_0 = 0.028 h^{-1} and λ_A = 0.74 h^{-1} μM^{-1} (continuous); λn_0 = 0.025 h^{-1} and λ_A = 0.668 h^{-1} μM^{-1} (constant). The coefficients of determination for the fits were R^2 = 0.94 (continuous) and 0.99 (constant). The similarity of parameter values is expected because these values are a property of the cell/drug combination and should be independent of time protocol of delivery. Also, the larger specific death rates found in these experiments are consistent with the observation that cell kill is achieved at smaller initial drug concentrations.

Prediction of Dose Response Curves. We used the average values of the specific death rate λ_A and uptake rate λn_0 calibrated (Figures 2,3; Supporting Information, Table S1, *Text*) from the time-dependent data of HCC cell viability at two values of initial drug concentration σ_0, and predicted theoretical dose–response curves spanning the full range of drug concentrations by numerically integrating eq 1a,b up to t = 24 h (Materials and Methods). A comparison of the theoretical and experimental dose response curves, that is, fraction of viable cells n/n_0 at t = 24 h *versus*

initial drug concentration σ_0, for free DOX and DOX-loaded protocells is reported in Figure 5 (coefficients of determination R^2 = 0.987, 0.991, and 0.996 for MDR cell line with free DOX, DOX-loaded protocells, and parental cell line with free DOX). The parameter values used were λ_A = 0.051 $(h\cdot\mu M)^{-1}$ and λn_0 = 0.19 h^{-1} (MDR with DOX-loaded protocells); λ_A = 0.025 $(h\cdot\mu M)^{-1}$ and λn_0 = 0.069 h^{-1} (MDR with free DOX); λ_A = 0.769 $(h\cdot\mu M)^{-1}$ and λn_0 = 0.069 h^{-1} (parental with free DOX). The ability to accurately predict the entire dose response curves from parameter fits based on using just two experimental concentration values, despite the nonlinear nature of drug response and without incorporating complicated kinetic arguments to describe cell death, provides further support to the mathematical model assumptions.

"Equivalence" between Free-Drug and Protocell Dose—Response Curves. We further validated the mathematical model by demonstrating equivalence between free DOX and DOX-loaded HCC dose response (Figure 5, inset), by superposing least-squares fits through the two sets of dose—response data (rescaling the initial drug concentration σ_0 for the free-drug case by a factor of roughly 1/5 determined empirically). This remarkable result validates the mathematical model prediction (Materials and Methods) that differences in drug response corresponding to different experimental conditions of drug uptake and cell death can be accounted for through different values of the associated rate parameters in the model (Figure 3), while the fundamental functional relationships, for example, eq 1 between dose and response, universally apply to all cell and drug types, delivery time-courses, and delivery vehicles, that is, free drug *versus* protocells. For the case where DOX-loaded protocell and free DOX delivery are compared, the results in Figure 5 imply that the delivery of DOX using protocells is more efficient (because of higher cellular uptake rates) and affords a kill equal to the kill achieved by delivery of free DOX at a higher total concentration or at a later time.

Model Implications. We demonstrated the general applicability and predictive power of the mathematical model presented here by applying it to different cell and drug types, and to both free and nanocarrier-mediated drug delivery. Actually, this general modeling approach based on conservation laws has been successfully applied to the prediction of patient-specific response to drug and of response to immunotherapy in mice.[19,20] To date, extensive research has been conducted to study the drug delivery capabilities of nanoparticles compared to the traditional methods of delivery.[2,21,22] It has been shown that nanoparticles loaded with drugs are often superior in reaching intended targets than other approaches. Here we sought to understand the mechanisms underlying how the delivery of DOX and other drugs to HCC tumor cells using the protocell drug delivery vehicle results in more efficient and effective cell death than traditional free-DOX delivery. We found that this outcome primarily occurs because the protocell delivery allows the cells to uptake the drug at higher rates, which then leads to faster rates of death. The initial concentration of DOX σ_0 necessary to obtain the same amount of cell kill is less for protocell-mediated delivery compared to free-DOX delivery. This warrants the use of protocells as a viable alternative in the clinical setting. The ability of the protocells to circumvent or overcome the drug resistant pumps[5] within the cells and to be loaded with extremely high concentrations of DOX allows them to outperform free drug and other nanocarriers.

The two model parameters, that is, the integrated history of drug uptake by the cells over time of exposure and the uptake rate, sum up all higher-order phenomena (such as endosomal escape efficiency of the protocells *etc.*) that potentially play a role in determining drug response. Accordingly, these phenomena are not directly modeled in the mathematical formulation, as the two parameters are instead directly measured from "calibration" experiments as described throughout (see especially Figure 2 and associated text). We have also demonstrated that (see, *e.g.*, Figure 3), as a result of a number of higher-order phenomena, accounted for by different values of the two parameters, nanoparticle-based delivery leads to higher uptake rates and thus higher cell kill than free-drug delivery. Direct incorporation of higher-order mechanisms could in principle lead to an "*ab-initio*" predictive model that would potentially not require calibration. Furthermore, the protocell platform incorporates two pH-sensitive triggers that help to very efficiently deliver drug into the cytoplasm. First, acidification of the endosome destabilizes the supported lipid bilayer allowing drug escape and, second, the fusogenic peptide incorporated in the supported lipid bilayer serves as a proton sponge leading to endosome swelling and disruption. Together these triggers help to rapidly deliver the drug into the endosome so that endosomal escape efficiency is not in any way rate limiting and does not need to be specifically accounted for in the model as presented here.

CONCLUSIONS

Over 70 years of chemotherapy research have resulted in phenomenological explanations of cell death, typically confined to specific cell and drug types, but have failed to provide a unified mechanistic understanding of how underlying biophysical processes affect drug uptake and cellular death rates. We present a universal solution of first-principle conservation equations of cell and drug mass, incorporating the fundamental biological hypothesis that the history of drug uptake by the cells is the sole determinant of death rates. This general mathematical model

quantifies and predicts *in vitro* dose response of different human tumor types to a variety of drugs, elucidates the advantages of targeted nanoparticle-based drug delivery directly to cancer cells, and will help in the rational design of nanocarriers and drug dosing regimens.

MATERIALS AND METHODS

Experimental Determination of Dose–Response and Time-Dependent Viability in HCC Cells by Free Drug and Drug-Loaded Protocells. Detailed materials and methods that include procedures used to synthesize drug-loaded, SP94-targeted protocells have been published in the Supporting Information section of C. Ashley, *et al.*[5] Parental Hep3B (ATCC cat. no. HB-8064) were grown according to manufacturer instructions. MDR was induced *via* exposure to increasing concentrations of DOX in 24 h intervals (25, ..., 100, 150, ..., 500, 600, ..., 900 nM; 1, 1.5, ..., 3, 4, and 5 μM), interspersed with 48 h recovery periods, during which cells were incubated in complete growth medium without DOX.[23]

Dose–response curves for parental and MDR Hep3B, when exposed to free and protocell-encapsulated DOX, cisplatin, and 5-FU, were determined by seeding 6-well plates with 10^6 cells/well, allowing cells to adhere overnight, and then exposing cells to initial concentrations σ_0 = 0.1–10000 nM of drug in phenol red-free DMEM containing 10% or 50% FBS for 24 h at 37 °C. Here varying levels of serum were used to assess the stability of the protocells in complex media representative of *in vivo* environments. Cells that remained adherent were dislodged from the well using a cell scraper, centrifuged (4000 rpm, 2 min) to remove excess drug, and stained with SYTOX Green nucleic acid stain and Alexa Fluor 647-labeled annexin V. The numbers of viable (double-negative) and nonviable (single- or double-positive) cells were determined *via* flow cytometry (FACSCalibur); SYTOX Green fluorescence was excited by the 488-nm laser and collected in the FL1 channel, while Alexa Fluor 647 fluorescence was excited by the 633-nm laser and collected in the FL3 channel (670-nm long pass filter). The concentrations of drug necessary to kill 50% (LC_{50}) and 90% (LC_{90}) of cells were determined from the dose–response curves.

Time-response curves were then determined by continuously incubating cells with the LC_{50} or LC_{90} values of drug for 30 min to 72 h (continuous drug exposure). Discontinuous drug-exposure time-response curves were constructed by exposing cells to free or protocell-encapsulated drug up to t_d = 4 h and then incubating them in fresh medium for 30 min to 72 h. Cell viability was determined at various times points as described above. Parental and MDR Hep3B exposed to 1 μM of CsA for 72 h to reverse any Pgp-mediated resistance[24] were used as controls. The time-dependent viability and doubling rates of untreated cells were used to normalize all viability data.

Experimental Determination of Apoptosis in PANC-1 Cells by Free Gemcitabine. Cells were plated at a density of 5000 cells/well of a 96-well plate (Corning); 24 h after plating, the medium was replaced and gemcitabine was given at increasing concentrations σ_0 = 0, 3.1, 6.2, 12.5, 25, 50, 100, 500, and 1000 nM. Additionally, two experimental groups were tested at the same time. One group received only an initial dose of gemcitabine at one of the above concentrations (continuous drug exposure). Another group received one of the above concentrations of gemcitabine every 24 h, simulating a relatively "constant" exposure. Cell viability was determined with the MTS assay, according to manufacturer's protocol (Promega), at t = 1, 2, 24, 48, 72, and 96 h after initial gemcitabine exposure. All experiments were repeated three times.

We also used previously published data[17] of continuous DOX exposure of human breast cancer MCF-7 cells (both parental and MDR) to test the mathematical model. For these cells, as well as for the human pancreatic cancer PANC-1 cells exposed to gemcitabine as described below, dose–response data revealed the existence of a subpopulation of <10% of cells who were intrinsically resistant to the drugs used and survived at all drug concentrations applied. In the mathematical model analysis and for the purpose of comparing model results to *in vitro* viability data, these cells were removed from the analysis.

Mathematical Model of Coupled Cell and Drug Dynamics. The mathematical model from fundamental mass conservation considerations coupled with cytotoxicity monolayer data for protocells and free drug quantifies the advantages of the former nanocarrier drug delivery platform to tumor cells.

Equivalence of Dose–Response Curves. The drug concentration variable $\hat{\sigma}$ can be numerically eliminated from eqs 1a,b to obtain dose–response curves, that is, cell viability as function of initial drug concentration (through the parameter Φ) and time, $\hat{n} = F(\Phi,\hat{t})$. The functional form of F cannot be expressed analytically. This simple result demonstrates "equivalence" of dose–response curves corresponding to different values of drug uptake and cell death rate parameters particularly when these differences are due to different cell/drug types or delivery mechanisms, that is, nanocarriers *versus* free drug. Despite these differences, dose response is a universal function solely of dimensionless time $\hat{t}$ and the parameter Φ. Similar considerations apply to the other time-exposure courses considered eqs 2 and 3.

Calculation of Drug Concentration and Cell Viability. Here, the solutions of eq 1 were calculated by numerical integration of the corresponding differential eqs. S1–S4 (Supporting Information *Text*), using *Mathematica* (routine "NDSolve"),[25] and then fit to the cytotoxicity time-dependent data for continuous drug exposure of HCC cells at two different initial drug concentrations σ_0 for each cell type thus calibrating the death and uptake rate parameters Φ and λn_0, as shown in examples in Figure 2, where by fitting both the mean and the upper/lower bounds of the range of viability measurements at each concentration produced estimates of sensitivity of the model parameters (Figure 3; Supporting Information, Tables S1,S2, *Text*). Similar fits were performed for continuous drug-exposure to different drug types (Supporting Information *Text*).

Time dependent curves were also produced and compared to the discontinuous drug-exposure experiments with HCC cells by evaluating eq 2 using the same parameter values found from the fits described above for continuous exposure (Figure 4).

To predict dose–response curves for HCC cells (Figure 5), the parameter values found at two concentrations by the fits to the continuous drug-exposure data described above were then simply averaged; eq 1 was numerically evaluated at time t = 24 h for all concentrations σ_0 to produce the curves in Figure 5. A graph was then constructed by rescaling drug concentration to superpose dose–response data corresponding to free-drug and protocell delivery to demonstrate equivalence of the dose–response curves (Figure 5, inset). Equations 1 and 3 were also directly fitted at t = 96 h to dose–response data for MCF-7 breast cancer cell lines exposed continuously to DOX and to dose–response data for pancreatic adenocarcinoma PANC-1 cell lines exposed both continuously and to a constant concentration of gemcitabine, respectively, to produce the curves in Supporting Information Figure S1, *Text*.

Conflict of Interest: The authors declare no competing financial interest.

Supporting Information Available: A detailed description of the model derivation and additional results. This material is available free of charge *via* the Internet at http://pubs.acs.org.

Acknowledgment. P Dogra, A Day (Cristini lab); H Shen, M Ferrari (partial support for E.J.K.). Support: NIGMS K12GM088021 (J.P.); NSF Grant DMS-1263742, CTO PSOC-1U54CA143837, TCCN-1U54CA151668, USC PSOC-1U54CA143907, ICBP-1U54-CA149196 (V.C., Z.W.); NSF SBIR 1315372, the Victor and Ruby Hansen Surface Professorship in Molecular Modeling of Cancer (V.C.); Methodist Hospital Research Institute (E.J.K., V.C.); the Anne Eastland Spears Fellowship (E.J.K.); the Roadmap for Medical Research under Grant NIH PHS 2 PN2 EY016570B (C.J.B.),

NCI 1U01CA151792-01(E.C.C., C.J.B.), DOE BES Materials Science and Engineering Program (E.C.C., C.J.B.), Sandia National Laboratories LDRD (E.C.C., C.E.A., C.J.B.), NIEHS 1U19ES019528-01, NSF EF-0820117 (C.E.A., C.J.B.); the President Harry S. Truman Fellowship in National Security Science and Engineering at Sandia National Laboratories (C.E.A.).

REFERENCES AND NOTES

1. Chidambaram, M.; Manavalan, R.; Kathiresan, K. Nanotherapeutics to Overcome Conventional Cancer Chemotherapy Limitations. *J. Pharm. Pharm. Sci.* **2011**, *14*, 67–77.
2. Davis, M. E.; Chen, Z.; Shin, D. M. Nanoparticle Therapeutics: An Emerging Treatment Modality for Cancer. *Nat. Rev. Drug Discovery* **2008**, *7*, 771–782.
3. Torchilin, V. P. Recent Advances with Liposomes as Pharmaceutical Carriers. *Nat. Rev. Drug Discovery* **2005**, *4*, 145–160.
4. Ashley, C. E.; Carnes, E. C.; Epler, K. E.; Padilla, D. P.; Phillips, G. K.; Castillo, R. E.; Wilkinson, D. C.; Wilkinson, B. S.; Burgard, C. A.; Sewell, R. M.; *et al*. Delivery of Small Interfering RNA by Peptide-Targeted Mesoporous Silica Nanoparticle-Supported Lipid Bilayers. *ACS Nano* **2012**, *6*, 2174–2188.
5. Ashley, C. E.; Carnes, E. C.; Phillips, G. K.; Padilla, D.; Durfee, P. N.; Brown, P. A.; Hanna, T. N.; Liu, J.; Phillips, B.; Carter, M. B.; *et al*. The Targeted Delivery of Multicomponent Cargos to Cancer Cells by Nanoporous Particle-Supported Lipid Bilayers. *Nat. Mater.* **2011**, *10*, 389–397.
6. Liu, J.; Stace-Naughton, A.; Jiang, X.; Brinker, C. J. Porous Nanoparticle Supported Lipid Bilayers (Protocells) as Delivery Vehicles. *J. Am. Chem. Soc.* **2009**, *131*, 1354–1355.
7. El-Kareh, A. W.; Secomb, T. W. A Mathematical Model for Cisplatin Cellular Pharmacodynamics. *Neoplasia* **2003**, *5*, 161–169.
8. El-Kareh, A. W.; Secomb, T. W. Two-Mechanism Peak Concentration Model for Cellular Pharmacodynamics of Doxorubicin. *Neoplasia* **2005**, *7*, 705–713.
9. Gardner, S. N. A Mechanistic, Predictive Model of Dose–Response Curves for Cell Cycle Phase-Specific and -Nonspecific Drugs. *Cancer Res.* **2000**, *60*, 1417–1425.
10. Levasseur, L. M.; Slocum, H. K.; Rustum, Y. M.; Greco, W. R. Modeling of the Time-Dependency of *in Vitro* Drug Cytotoxicity and Resistance. *Cancer Res.* **1998**, *58*, 5749–5761.
11. Lankelma, J.; Fernández Luque, R.; Dekker, H.; Pinedo, H. M. Simulation Model of Doxorubicin Activity in Islets of Human Breast Cancer Cells. *Biochim. Biophys. Acta* **2003**, *1622*, 169–178.
12. El-Kareh, A. W.; Secomb, T. W. A Mathematical Model for Comparison of Bolus Injection, Continuous Infusion, and Liposomal Delivery of Doxorubicin to Tumor Cells. *Neoplasia* **2000**, *2*, 325–338.
13. Sanga, S.; Sinek, J. P.; Frieboes, H. B.; Ferrari, M.; Fruehauf, J. P.; Cristini, V. Mathematical Modeling of Cancer Progression and Response to Chemotherapy. *Expert Rev. Anticancer Ther.* **2006**, *6*, 1361–1376.
14. Sinek, J.; Frieboes, H.; Zheng, X.; Cristini, V. Two-Dimensional Chemotherapy Simulations Demonstrate Fundamental Transport and Tumor Response Limitations Involving Nanoparticles. *Biomed. Microdevices* **2004**, *6*, 297–309.
15. Sinek, J. P.; Sanga, S.; Zheng, X.; Frieboes, H. B.; Ferrari, M.; Cristini, V. Predicting Drug Pharmacokinetics and Effect in Vascularized Tumors using Computer Simulation. *J. Math. Biol.* **2009**, *58*, 485–510.
16. Eliaz, R. E. Determination and Modeling of Kinetics of Cancer Cell Killing by Doxorubicin and Doxorubicin Encapsulated in Targeted Liposomes. *Cancer Res.* **2004**, *64*, 711–718.
17. Frieboes, H. B.; Edgerton, M. E.; Fruehauf, J. P.; Rose, F. R.; Worrall, L. K.; Gatenby, R. A.; Ferrari, M.; Cristini, V. Prediction of Drug Response in Breast Cancer Using Integrative Experimental/Computational Modeling. *Cancer Res.* **2009**, *69*, 4484–4492.
18. van de Ven, A. L.; Wu, M.; Lowengrub, J.; McDougall, S. R.; Chaplain, M. A.; Cristini, V.; Ferrari, M.; Frieboes, H. B. Integrated Intravital Microscopy and Mathematical Modeling to Optimize Nanotherapeutics Delivery to Tumors. *AIP Adv.* **2012**, *2*, 11208.
19. Pascal, J.; Bearer, E. L.; Wang, Z.; Koay, E. J.; Curley, S. A.; Cristini, V. Mechanistic Patient-Specific Predictive Correlation of Tumor Drug Response with Microenvironment and Perfusion Measurements. *Proc. Natl. Acad. Sci. U.S.A.* **2013**, *110*, 14266–14271.
20. Das, H.; Wang, Z.; Niazi, M. K.; Aggarwal, R.; Lu, J.; Kanji, S.; Das, M.; Joseph, M.; Gurcan, M.; Cristini, V. Impact of Diffusion Barriers to Small Cytotoxic Molecules on the Efficacy of Immunotherapy in Breast Cancer. *PLoS One* **2013**, *8*, e61398.
21. Cho, K.; Wang, X.; Nie, S.; Chen, Z. G.; Shin, D. M. Therapeutic Nanoparticles for Drug Delivery in Cancer. *Clin. Cancer Res.* **2008**, *14*, 1310–1316.
22. Ferrari, M. Frontiers in Cancer Nanomedicine: Directing Mass Transport through Biological Barriers. *Trends Biotechnol.* **2010**, *28*, 181–188.
23. Minko, T.; Kopeckova, P.; Kopecek, J. Chronic Exposure to HPMA Copolymer-Bound Adriamycin Does Not Induce Multidrug Resistance in a Human Ovarian Carcinoma Cell Line. *J. Controlled Release* **1999**, *59*, 133–148.
24. Tong, A. W.; Su, D.; Mues, G.; Tillery, G. W.; Goldstein, R.; Klintmalm, G.; Stone, M. J. Chemosensitization of Human Hepatocellular Carcinoma Cells with Cyclosporin A in Post-Liver Transplant Patient Plasma. *Clin. Cancer Res.* **1996**, *2*, 531–539.
25. *Mathematica, Mathematics and Algorithms*, version 8.0; Wolfram Research: Champaign, IL, 2008; http://www.wolfram.com/learningcenter/tutorialcollection/MathematicsAndAlgorithms/MathematicsAndAlgorithms.pdf.